https://doi.org/10.5194/amt-2020-313
Preprint. Discussion started: 15 September 2020

Atmospheric Measurement Techniques Discussions

Measurements of atmospheric He/N_2 as an indicator of fossil fuel extraction and stratospheric circulation

Benjamin Birner[1], William Paplawsky[1], Jeffrey Severinghaus[1], and Ralph F. Keeling[1]

[1]Scripps Institution of Oceanography, UC San Diego, La Jolla, CA 92093, USA

Correspondence to: Benjamin Birner (bbirner@ucsd.edu)

Abstract. The atmospheric He/N_2 ratio is expected to be increasing due to the emission of He associated with fossil fuels and is expected to also vary in both space and time due to gravitational separation in the stratosphere. These signals may be useful indicators of fossil-fuel exploitation and variability in stratospheric circulation, but direct measurements of He/N_2 ratio are lacking on all time scales. Here we present a high-precision custom inlet system for mass spectrometers that continuously stabilizes the flow of gas during sample-standard comparison and removes all non-noble gases from the gas stream, enabling unprecedented accuracy in measurement of relative changes in the $^4He/N_2$ ratio. Repeat measurements of the same combination of high-pressure tanks using our inlet system achieves a reproducibility of ~10 per meg (i.e. 0.001%) in 6–8h analyses. This compares to interannual changes of He/N_2 gravitational enrichment at ~35 km in the mid latitude stratosphere of order 300–400 per meg, and an annual tropospheric increase from human fossil fuel activity of less than ~30 per meg y^{-1} (bounded by previous work on helium isotopes). The gettering and flow-stabilizing inlet may also be used for the analysis of other noble gas isotopes and could resolve previously unobserved seasonal cycles in Kr/N_2 and Xe/N_2.

1 Introduction

The atmospheric mole fraction of helium in dry air is typical ~5.24 ppm (Glückauf, 1944) with an isotopic abundance of ^4He about 10^6 times greater than ^3He. On geological time scales, the natural concentration of ^4He in the atmosphere is set by a balance of ^4He loss to space and ^4He release from the Earth's crust, where it is produced by radioactive decay of uranium and thorium (Kockarts, 1973; Pierson-Wickmann et al., 2001; Sano et al., 2013; Torgersen, 1989; Zartman et al., 1961). Over the past century, human exploitation of fossil fuels likely has accelerated the release of crustal He, but the observational evidence of a secular increase of atmospheric ^4He remains ambiguous presumably due to a lack of analytical precision (Boucher et al., 2018c; Lupton and Evans, 2013, 2004; Mabry et al., 2015; Oliver et al., 1984; Pierson-Wickmann et al., 2001; Sano et al., 1989). Additionally, recent measurements and model simulations reveal a small depletion of gases heavier than air in the stratosphere by gravitational separation (Belikov et al., 2019; Birner et al., 2020; Ishidoya et al., 2020, 2018, 2013, 2008; Sugawara et al., 2018) suggesting a corresponding enrichment of the light gas helium. Gravitational separation is only partially counteracted by the large-scale stratospheric circulation and mixing, which tends to homogenize the atmosphere. Variability

https://doi.org/10.5194/amt-2020-313
Preprint. Discussion started: 15 September 2020

in stratospheric circulation and stratosphere-troposphere exchange (STE) could therefore impact the degree of fractionation and cause additional interannual changes in the stratospheric and, to a much lesser extent, the tropospheric abundance of ^4He. Measurements of He/N_2 may provide an alternative indicator of variations in stratospheric circulation and STE. An improved understanding of STE is critical because stratospheric circulation changes affect tropospheric trends of societally-important trace and greenhouse gases such as N_2O, CH_4, ^{14}C, O_3 and CFCs (Arblaster et al., 2014; Graven et al., 2012; Hamilton and Fan, 2000; Hegglin and Shepherd, 2009; Montzka et al., 2018; Nevison et al., 2011; Simmonds et al., 2013). These gases all have significant sources or sinks in the stratosphere that cause strong stratosphere-troposphere concentration differences. Global circulation models consistently predict an acceleration of the stratospheric Brewer-Dobson Circulation (BDC; Brewer, 1949; Dobson, 1956) under global warming (Butchart, 2014). Stratospheric circulation is also naturally modulated on a range of shorter time scales from synoptic-scale events to decadal variations (e.g., Holton et al., 1995; Li et al., 2012; Flury et al., 2013; Butchart, 2014; Ray et al., 2014). Circulation changes have typically been observed using measurements of numerous different trace gases in the stratosphere (e.g., CO_2, SF_6, H_2O, O_3, CO, or N_2O) (e.g., Bönisch et al., 2009; Engel et al., 2009, 2017; Ray et al., 2010; Haenel et al., 2015). However, interpretation of these tracers of stratospheric circulation is complicated by complex chemical source and sink processes, whereas gravitational fractionation of He/N_2 is governed by comparatively simple physics.

Atmospheric He/N_2 measurements may also provide an indication of the history of fossil-fuel usage. Previous attempts to measure the fossil-fuel signal in He has centered on measurements of changes in the atmospheric $^3He/^4He$ isotope ratio (Boucher et al., 2018c; Lupton and Evans, 2013, 2004; Mabry et al., 2015; Oliver et al., 1984; Sano et al., 1989). However, measurements of the $^3He/^4He$ ratio are fundamentally limited by the extremely low abundance of ^3He (e.g., Mabry et al., 2015; Boucher et al., 2018b), with only 1 in 730,000 He atoms being ^3He. Therefore, the precision on individual $^3He/^4He$ analyses is limited to ~±0.2%. This is insufficient for the detection of the stratospheric and anthropogenic signals we are interested in, and which we estimate to cause variations in the atmospheric ^4He mole fraction on the order of 0.0030 to 0.04% y^{-1} (see section 2.1 & 2.2.). Moreover, small changes in ^3He from radioactive decay of tritium in nuclear warheads may complicate the interpretation of $^3He/^4He$ results (e.g., Christine Boucher et al., 2018c; Lupton and Evans, 2004).

Here we describe a method to measure relative differences in ^4He mole fraction ($^4He/M$) between two large samples of air using a custom mass spectrometer inlet system. The helium mole fraction can later be mathematically translated to our target ratio, $^4He/N_2$, given supplementary measurements of O_2, Ar, and CO_2 (see discussion). This is advantageous because N_2 is near-constant in the atmosphere making $^4He/N_2$ more readily interpretable than $^4He/M$. The $^4He/M$ method depends on stabilization of the gas flow to the ion source between a sample and standard gas to achieve high precision differencing. Novel elements in our setup include continuous flow removal of reactive gases via titanium gettering immediately upstream of the mass spectrometer inlet, and the use of an actively-controlled open split (Henneberg et al., 1975) for balancing pressures upstream of a shared capillary directed towards the mass spectrometer. Gas handling techniques, the inlet system and the continuous-flow getter oven are described in detail below.

https://doi.org/10.5194/amt-2020-313
Preprint. Discussion started: 15 September 2020

Atmospheric Measurement Techniques Discussions

1.1 Gravitational fractionation of He/N_2 in the stratosphere

The notion that the stratospheric and tropospheric He/N_2 ratio must vary in response to fluctuations in stratospheric circulation is based on studies of the atmospheric Ar/N_2 ratio (Birner et al., 2020; Ishidoya et al., 2020). Relative changes in the Ar/N_2 ratio (or He/N_2) are commonly expressed in delta notation:

$$\delta(Ar/N_2) = \frac{\left(\frac{Ar}{N_2}\right)_{SA}}{\left(\frac{Ar}{N_2}\right)_{ST}} - 1 \tag{1}$$

where subscripts SA and ST refer to the ratio in a sample and a reference gas mixture, respectively. $\delta(Ar/N_2)$ is multiplied by 10^6 and expressed in "per meg" units.

Sensitivity tests with the 2-D chemical-dynamical-radiative model of the atmosphere SOCRATES by Ishidoya et al. (2020) indicate that significant temporal changes in stratospheric Ar/N_2 should occur in response to an acceleration or deceleration of the BDC. The simulations also suggest a weak stratospheric influence on tropospheric Ar/N_2. Ishidoya et al find that imposing a gradual acceleration of the BDC of 4% dec^{-1} leads to a 40 per meg dec^{-1} increase in $\delta(Ar/N_2)$ at ~35 km altitude in northern mid-latitudes, and a corresponding 1.3 per meg dec^{-1} decrease of $\delta(Ar/N_2)$ in the troposphere. Furthermore, they find that imposing 3-year periodic changes of 10% in BDC yields anomalies of ±25 and ±0.4 per meg in stratospheric and tropospheric $\delta(Ar/N_2)$, respectively. Tropospheric observations of $\delta(Ar/N_2)$ by Ishidoya et al. (2020) would be consistent with larger STE-induced interannual changes of tropospheric Ar/N_2. Variability of the BDC on the order of 10% or more on seasonal to decadal time scales is consistent with published estimates (Flury et al., 2013; Ray et al., 2014; Salby and Callaghan, 2006).

The atmospheric He/N_2 ratio must be more strongly impacted by gravitational fractionation than Ar/N_2 due to the larger mass difference and higher diffusivity of He than Ar, which brings He closer to gravitational equilibrium. The gravitational fractionation effect on He/N_2 can be scaled from Ar/N_2 (Birner et al., 2020) using the molar mass difference to air ΔM_i ($\Delta M_i = M_i - 0.02896$ kg mol^{-1}) and the molecular diffusivity D_i of gas i in air as:

$$\delta(\mathrm{He/N_2}) = \frac{\left(\frac{He}{N_2}\right)_{SA}}{\left(\frac{He}{N_2}\right)_{ST}} \approx \frac{D_{He}^{air}\Delta M_{He} - D_{N2}^{air}\Delta M_{N2}}{D_{Ar}^{air}\Delta M_{Ar} - D_{N2}^{air}\Delta M_{N2}}\delta(\mathrm{Ar/N_2}). \tag{2}$$

Using the method of Fuller et al. as reported in (Reid et al., 1987), D_{He} is 3.6 times greater than D_{Ar} and ΔM is more than twice as large, making $\delta(He/N_2)$ ~7.5 times more strongly fractionated by gravity than $\delta(Ar/N_2)$ in the stratosphere.

1.2 Other controls on tropospheric He/N_2

A variety of known natural processes influence tropospheric $^4He/N_2$ is summarized in Figure 1 and Table 1. Natural ^4He release from the Earth's crust is mediated by volcanism, ground water discharge and diffusive leakage. At the same time, helium is

https://doi.org/10.5194/amt-2020-313
Preprint. Discussion started: 15 September 2020

lost to space by thermal and non-thermal escape (Kockarts, 1973; Oliver et al., 1984; Pierson-Wickmann et al., 2001; Sano et al., 2013; Torgersen, 1989). Based on these natural fluxes and the total atmospheric burden, the atmospheric residence time of ^{4}He is estimated to be ~1 million years.

Over the few last centuries, He release from fossil-fuel extraction has dwarfed the natural release rates of ^{4}He by several orders of magnitude. Based on knowledge of fossil fuel usage and He content of the material (Table 1) the additional ^{4}He release rate is estimated to be of order 3 to 30×10^{10} mole yr^{-1} (e.g., Oliver et al., 1984; Sano et al., 1989, 2013; Pierson-Wickmann et al., 2001) implying that ^{3}He/^{4}He should be decreasing at rates between 35 and 350 per meg y^{-1}. However, in contrast to these predictions and some earlier observations (Oliver et al., 1984; Pierson-Wickmann et al., 2001; Sano et al., 2010, 1989), no significant trend in atmospheric ^{3}He/^{4}He has been observed using archived air samples spanning from the beginning of the 20th century to today at the level of roughly ±30 per meg per year, suggesting similarly small increase rates in δ(He/N_2) (Boucher et al., 2018c; Lupton and Evans, 2013, 2004; Mabry et al., 2015).

He release from fossil-fuel extraction is also expected to impose an interhemispheric gradient in δ(He/N_2). A rough upper bound can be estimated by assuming all fossil-fuel derived He emissions occur in the Northern Hemisphere and interhemispheric mixing of the atmosphere has a time scale of about one year. This would yield a north-south difference of 30 per meg, equal to the expected annual rise in δ(He/N_2).

Seasonal and long-term ocean warming can cause small changes in He/N_2, mainly due to the impact on N_2. From observations of δ(Ar/N_2) (Keeling et al., 2004) and solubility data of Ar, He and N_2 (Hamme and Emerson, 2004; Weiss, 1971), we estimate that the impact on He/N_2 of air-sea exchanges is on the order of 0.16 per meg y^{-1} for the secular ocean warming trend and 3-9 per meg for seasonal heat exchanges. Therefore, the ratio of stratospheric signals to ocean warming is ~12 times greater for He/N_2 than Ar/N_2 and the effect of slow ocean warming is over two orders of magnitude smaller than the influence of fossil fuel exploitation.

The He/N_2 ratio could also be impacted by processes changing atmospheric N_2. However, the annual removal of 7.5x10^{12} moles N_2 y^{-1} by anthropogenic nitrogen fixation in agriculture, combustion, and industry is clearly negligible compared to the ~1.4x10^{20} moles of N_2 in the whole atmosphere (Fowler et al., 2013). Volcanic emissions of N_2 are likewise negligible, order 10^9 moles y^{-1}.

2 Methods

Our He/N_2 analysis method relies on measuring the helium mole fraction relative difference between an air sample and a standard reference gas using a single collector for $^4He^+$ on a magnetic sector mass spectrometer (MS). Crucially, whole dry air is pressure-stabilized to a high level prior to gettering, so that the beam intensity ratio being measured is effectively the ^{4}He to air ratio. Measurements of the He mole fraction difference can also be expressed similarly to Eq. (1) as δ(^{4}He/M) where M is total moles. By applying small corrections for variations in O_2/N_2, Ar/N_2, and CO_2, the quantity δ(^{4}He/M) is easily related to δ(^{4}He/N_2).

https://doi.org/10.5194/amt-2020-313
Preprint. Discussion started: 15 September 2020

The MS is interfaced to a custom inlet system with on-line gettering and active flow stabilization using an actively pressure-controlled open split (Henneberg et al., 1975), as shown in Figure 2.

2.1 The Inlet system

The design of the inlet system incorporates elements of an open split (Henneberg et al., 1975) but further stabilizes the pressure using active control elements and allows active switching between a sample (SA) and reference standard gas stream (ST). Pneumatically-actuated pistons (Fig. 2C) alternately slide 0.3-mm tubes exhausting sample or standard gas close to a shared intake capillary which is placed at the end of the stabilization chamber (Fig. 2D) and connects the chamber to the getter oven and MS. The chamber is shaped as a funnel to guide the sliding tubing into a reproducible resting position. Variations in chamber pressure are measured with a 0.2-Torr MKS 223B differential pressure gauge and are limited to better than 1 part in 10^6 by opening an MKS Type 248 Control Valve which allows most of the gas in the stabilization chamber to be pumped away by a vacuum pump. The valve is controlled via an MKS 250E Control Module. The 0.3mm tubes enter the chamber through sliding seals lubricated with vacuum grease, thus allowing the chamber to be operated at a selected pressure above or below ambient. The default setting is 14 psia (96.5 kPa). The shared outlet capillary is crimped and thermally insulated. The pressure in the getter oven (Fig. 2E) is about 2 mTorr (0.3 Pa) because the getter material effectively acts as a vacuum pump.

2.2 Continuous-flow gettering

In the getter chamber (Fig. 2E), high purity titanium sponge (Ti) irreversibly reacts with N_2, O_2, CO_2, and other non-noble gases in air to form titanium nitride (TiN), titanium dioxide (TiO_2), titanium carbide (TiC) and other compounds at ~850°C. This increases the concentration of He in the gas mixture by a factor of about 100, boosting precision. The getter oven is manufactured from heat resistant stainless steel (SS310) and equipped with VCR face seals for easy maintenance. The temperature of the getter oven is determined by manually adjusting the power provided to the furnace surrounding the getter. The furnace is additionally equipped with an independent limit controller for safety.

The gettering efficiency depends on the furnace's temperature and must be balanced against material tolerance and increased evolution of H_2 gas from the metal in the getter. H_2 forms a solid solution in Ti and is continuously released to the gas stream when Ti is heated. The solution process is reversible and H_2 is absorbed if the Ti is cooled down. H_2 could interact with He^+ in the source or combine with ionized gas to form hydride compounds such as ArH^+ (Fig. 3) However, since the H_2 flux into the gas stream varies slowly compared to the 30-second switching timescale, the impact of H^+ cancels during sample-standard comparison. In its current size (~10–12 g Ti), the getter can be used for 70–80 h before the Ti must be replaced. This requires breaking vacuum in the inlet approximately once every four weeks depending on usage. After replacement, fresh titanium is gradually heated to 900°C over ~12h in isolation from the MS to allow degassing without contaminating the MS. A coarse mesh of metal wire and 2 μm SWAGELOK filters on both sides of the getter prevent getter-derived dust from entering the vacuum system and MS.

https://doi.org/10.5194/amt-2020-313
Preprint. Discussion started: 15 September 2020

Atmospheric Measurement Techniques Discussions

2.3 Inlet operation

We have developed customized scripts using the software ISODAT provided with any MAT253 mass spectrometer to control the inlet system and operate the pneumatic actuators for He/M analysis (Fig. 3). In a typical run, the instrument performs sample-standard gas switching with a ~30 second switching time (~60 sec full cycle), using a conservative 18-second idle time to ensure complete flush-out of the stabilization chamber and the getter oven. As customary in dynamic MS noble gas application, we group each analysis into blocks consisting of (i) adjusting the accelerating voltage to find the center of the ^4He peak followed by (ii) 20 sample-standard comparisons. Background concentrations of ^4He in the MS are determined daily and subtracted. Data are quality controlled and anomalous cycles are rejected when delta values deviate by more than 3 standard deviations from the smoothed time series or when there are abrupt changes detected in the ion beam associated with instability in the MS source (not shown). ISODAT also monitors the MS source pressure and closes the external change-over-valve (Fig. 2) to protect the MS in case of a pressure control failure.

2.4 Gas handling and sample delivery systems

Air can be delivered to the inlet system from either a pair of high-pressure gas cylinders (Fig. 2A) or from a continuous-flow system (Fig. 2B) pumping locally-sampled ambient air directly to the laboratory. For He/N_2 reference material, we rely on compressed dry air stored in high pressure cylinders, as is conventional for atmospheric measurements of O_2/N_2, CO_2, and Ar/N_2 (Keeling et al., 2007). All cylinders are stored horizontally for 2 days in a thermal enclosure before analysis to minimize the risk of thermal fractionation. The pressure is dropped to slightly above ambient directly at the head valve of high-pressure cylinders using capillaries rather than regulators. The use of capillaries ensures that all wetted parts are exclusively metal, which is impermeable to He, and eliminates problems we encountered using regulators during initial tests. Due to the use of capillaries, the gas delivery system cannot be evacuated efficiently and instead must be purged for several hours ahead of analysis until the signal stabilizes. The flow rates in the lines are monitored using 0.1l Omron DF6-P flow meters and are manually balanced at around 27-28 cm^3 min^{-1} before every analysis by adjusting the crimping of the capillaries. Sample and standard gas streams each flow through a -80°C cold trap made from 1/4" stainless steel tubing before entering the pressure stabilization chamber (Fig. 2D).

3 Results

3.1 Gettering performance

A mass scan of medical air introduced through the gettering and flow-stabilizing inlet system revealed that N_2 and O_2 are almost completely removed from the air by the on-line getter (Fig. 4). ^{40}Ar ions with one or more charges yield the largest beams in the scan followed by ^{36}Ar, and H_2 evolving from the hot metal in the getter oven.

https://doi.org/10.5194/amt-2020-313
Preprint. Discussion started: 15 September 2020

Atmospheric Measurement Techniques Discussions

3.2 Response time

Our setup demonstrates the ability to transition between sample and standard gas with a e-folding time scale of ∼4 seconds (Fig. 5). The e-folding time is primarily controlled by the volume of the getter and the total flow of gas through the getter. Regions of the inlet system upstream of the getter experience ~100x faster flushing than downstream of the getter because the gas upstream still contains N_2 and O_2 and hence flows much faster. The e-folding time does not change substantially over the life span of the getter.

3.3 Analytical precision

Using the default 60 sec sample-standard cycle, the gettering and flow-stabilizing inlet system achieves an internal precision in δ(He/M) of approximately ±15 per meg over 1.5h and ±8 per meg (1σ) for samples run 6h or longer (Figs. 6&7). The reproducibility of repeated 6–8h measurements of the same sample and standard gas cylinder combination is comparable and essentially as expected from the shot-noise on the ^{4}He ion current.
The zero enrichment, i.e., the delta value observed when introducing the same gas through sample and standard side of the inlet, is generally small and stable over time. It is tested by mounting the crimped delivery capillaries (Fig. 2A) to a tee fitting, which splits the gas stream at high pressure from a single tank of air. This tee minimizes thermal fractionation by dividing the flow at a junction machined into the center of a large brass block (Keeling, 1988). Identical delta values (within error) obtained after reversing the outlet from the tee demonstrate that no measurable fractionation occurs within the tee and therefore that the zero enrichment reflects a persistent asymmetry somewhere downstream, most likely within the open split. The typical zero enrichment varies slightly with the mean flow of gas into the stabilization chamber (F), the pressure in the chamber (P), and the flow offset between SA and ST side (ΔF) before entering the stabilization chamber (Fig. 7). Weighted multiple linear regression analysis using 3 different pressure levels (9 psi, 14 psi, and 16 psi, i.e, 62.1, 96.5, and 110.3 kPa) reveals that the zero enrichment value decreases by 2.8±0.9 per meg per 1 cm^3 min^{-1} change in mean flow away from 27.5 cm^3 min^{-1} and increases by 17.2±4.8 per meg per 1 cm^3 min^{-1} flow imbalance between SA and ST. The dependence of δ(He/M) on F and ΔF is significant at the 5% level. For a balanced flow of 27.5 cm^3 min^{-1} at 9, 14 and 16 psi pressure in the stabilization chamber, the mean zero enrichment is -9.61±7.2 per meg, 1±3.7 per meg and -15.7±4.7 per meg, respectively. P is held constant for measurements at 14 psi. F and ΔF are stable over 8h to within ±0.2 cm^3 min^{-1}. This typically yields a correction for mean gas flow and flow imbalance of less than 10 per meg with an uncertainty smaller than 6 per meg, which increases the overall analytical uncertainty in repeat tank analysis from 8 to 10 per meg.

https://doi.org/10.5194/amt-2020-313
Preprint. Discussion started: 15 September 2020

4 Discussion

The gettering and flow-stabilizing inlet system has demonstrated the ability to determine the helium mole fraction difference between a sample and standard gas, δ(He/M), to about 10 per meg in a single 6–8h analysis. δ(He/M) can be related to $\delta(He/N_2)$ using

$$\delta(He/N_2) \simeq \delta(He/\mathrm{M}) + \delta(O_2/N_2)X_{O_2} + \delta(Ar/N_2)X_{Ar} + dX_{CO_2} \quad (1)$$

as derived in Box 1, using independent measurements of $\delta(O_2/N_2)$, $\delta(Ar/N_2)$, and dX_{CO2} (Keeling et al., 2004, 1998). These corrections are relatively small and therefore do not significantly contribute to the overall uncertainty of $\delta(He/N_2)$. The long-term atmospheric changes in $\delta(O_2/N_2)$ ~ -19 per meg yr^{-1} and dX_{CO2} ~2.5 ppm yr^{-1} yield corrections of approximately -4 per meg yr^{-1} and +2.5 per meg yr^{-1}, respectively. The seasonal variations in $\delta(O_2/N_2)X_{O2}$ and dX_{CO2} partly cancel, yielding net seasonal corrections of ~10 per meg in both hemispheres. The term $\delta(Ar/N_2)X_{Ar}$ contributes variations less than 1 per meg on all time scales.

Box 1. Deriving the helium-to-nitrogen ratio from δ(He/M)

A relationship between $\delta(He/N_2)$ and δ(He/M) can be derived from:

$$\delta(He/N_2) = \frac{dHe}{He} - \frac{dN_2}{N_2} = \frac{dHe}{He} - \frac{dM}{M} - \frac{dN_2}{N_2} + \frac{dM}{M} = \delta(He/\mathrm{M}) - \frac{dN_2}{N_2} + \frac{dN_2 + dO_2 + dAr + dCO_2}{M}$$

Using $\frac{dN_2}{\mathrm{M}} = \frac{dN_2}{N_2} X_{N_2}$, $\frac{dO_2}{\mathrm{M}} = \frac{dO_2}{O_2} X_{O_2}$, etc, where X_i is the mole fraction of gas i, yields

$$\delta(He/N_2) = \delta(He/\mathrm{M}) + \frac{dN_2}{N_2}\left[-1 + X_{N_2} + X_{O_2} + X_{Ar} + X_{CO_2} + X_{H_2O} \ldots\right] + \left[\frac{dO_2}{O_2} - \frac{dN_2}{N_2}\right]X_{O_2} + \left[\frac{dAr}{Ar} - \frac{dN_2}{N_2}\right]X_{Ar} + \left[\frac{dCO_2}{CO_2} - \frac{dN_2}{N_2}\right]X_{CO_2} + \cdots$$

This can be simplified to Eq. (3) using $\left[\frac{dCO_2}{CO_2} - \frac{dN_2}{N_2}\right]X_{CO_2} = dX_{CO_2}$, which follows because relative changes in CO_2 are much larger than relative changes in N_2.

4.1 Potential applications

The presented He/N_2 measurement capability has a range of possible applications. Our primary targets are (i) to use stratospheric $\delta(He/N_2)$ as a tracer of the large-scale stratospheric circulation and (ii) to evaluate tropospheric $\delta(He/N_2)$ trends as a possible indicator of anthropogenic fossil fuel exploitation.

We expect an excellent signal-to-noise ratio for the detection of stratospheric changes in $\delta(He/N_2)$. Interannual variability in stratospheric $\delta(He/N_2)$ is likely on the order 300–400 per meg (Table 1). Repeat 6–8h measurements of a high-pressure tank currently achieve a precision of ~10 per meg, or about 40 times better than the stratospheric signal. Associated changes in tropospheric $\delta(He/N_2)$, in contrast, are likely much smaller at around 6 per meg and therefore at or below the current limit of

https://doi.org/10.5194/amt-2020-313
Preprint. Discussion started: 15 September 2020

detection even after averaging of multiple samples. The reproducibility of measurements also depends on adequate calibration strategies. The short-term reproducibility of high-pressure cylinders shown in Figure 6 and the long-term stability established for O_2/N_2, CO_2, and Ar/N_2 standard gases in previous work (Keeling et al., 2007) suggest long-term stability in $\delta(He/N_2)$ is achievable but needs further evaluation.

He/N_2 measurements can help quantify the anthropogenic ^4He release over time due to fossil fuel extraction (Boucher et al., 2018c; Lupton and Evans, 2013, 2004; Mabry et al., 2015; Oliver et al., 1984; Sano et al., 2010, 1989). Although theoretical predictions clearly support an anthropogenic ^4He increase, past observational studies produced conflicting evidence. Recent improvements in analytical methods and sampling have narrowed the uncertainty in $^3He/^4He$ trend estimates to <30 per meg y^{-1} with a mean statistically indistinguishable from zero (Table 1). However, with a precision of ~10 per meg on single samples, measurements of $\delta(^4He/N_2)$ on decades-old archived air may allow trend detection to ~1 per meg y^{-1} or better, while also avoiding possible complications from ^3He emissions.

Another possible application is the investigation of spatial gradients in atmospheric $\delta(He/N_2)$ caused by the distribution of local volcanic or anthropogenic sources (e.g., Sano et al., 2010; Boucher et al., 2018c). High precision $\delta(He/N_2)$ may allow the detection of diffuse helium release in regions of volcanic activity (Boucher et al., 2018b). Furthermore, global north-south $\delta(He/N_2)$ gradients from anthropogenic emission sources concentrated in the Northern Hemisphere are likely on the order of 10s of per meg and thus may also be detectable directly. Alternatively, studies could target more local gradients around oil or natural gas facilities that are likely even greater.

The method developed here is potentially applicable to measure the abundance of any noble gas in air. The intensity of the ion beam and thus the precision for different noble gases depends on their natural abundance and ionization efficiency in the MS source. ^{20}Ne and ^{22}Ne have isobaric interferences from doubly charged Ar and CO_2, but Kr and Xe yield usable ion beams (Table 2). We estimate a precision of ~5 and ~19 per meg for repeat 6–8h analyses of $\delta(^{84}Kr/^{28}N_2)$ and $\delta(^{129}Xe/^{28}N_2)$ respectively, by assuming that precision scales with the square root of the total ions counted as expected from shot-noise behavior. This estimate compares favorably to the precision currently reported in conventional dual inlet mass spectrometry studies (Baggenstos et al., 2019; Bereiter et al., 2018). For example, Baggenstos et al. (2019) achieved a precision of 88 per meg and 203 per meg for repeat ~2h analyses of $\delta(^{84}Kr/^{40}Ar)$ and $\delta(^{132}Xe/^{40}Ar)$ in ambient air, respectively.

The improved precision enabled by our inlet system should be sufficient to resolve the previously unobserved annual cycle of Kr and Xe caused by the seasonal release and uptake of both gases by the ocean as it warms and cools. The seasonal cycle of $\delta(^{40}Ar/^{28}N_2)$ has an amplitude of 5–15 per meg in the extratropics (Keeling et al., 2004). $\delta(^{84}Kr/^{28}N_2)$ and $\delta(^{132}Xe/^{28}N_2)$ however are ~3.4 and ~8.9 times more sensitive than $\delta(^{40}Ar/^{28}N_2)$ to changes in ocean temperature owing to the different temperature-dependences of Ar, Kr and Xe solubility in seawater (Hamme and Emerson, 2004; Jenkins et al., 2019). This implies that seasonal variations in $\delta(^{84}Kr/^{28}N_2)$ and $\delta(^{132}Xe/^{28}N_2)$ have a magnitude of 17–51 and 45–134 per meg respectively, which would be readily resolved if precision of our system scales as expected with signal strength.

The gettering inlet and MS system was applied here only for single ion (He^+) detection, but alternately could be applied for multi-ion collection. The acquisition of Kr and Xe isotope ratios for example would provide valuable additional information for detecting artefactual fractionation during sampling and allow further improvements in precision by increasing the total number of ions collected.

The need for only a single ion detector also allows the gettering and flow-stabilizing inlet to be interfaced with simpler and more affordable mass spectrometers, such as quadrupole systems. The performance of the system will depend on the stability of the $^4He^+$-ion beam over the time scale of switching and will need to be evaluated critically, but any variability on time scales longer than the switching time is canceled by sample-standard differencing.

5 Conclusions

Here, we presented a new method for high-precision measurements of changes in the He/N_2 ratio of atmospheric air. The method relies on monitoring of the $^4He^+$ ion beam in a mass spectrometer during sample-standard switching. The ion beam is stabilized by flowing sample and standard air through a single capillary into the MS from an actively pressure-controlled open-split (Henneberg et al., 1975), such that variability of the $^4He^+$ ion beam directly reflects differences in the helium mole fraction of the gas mixtures. Measurements of the helium mole fraction can easily be converted to $\delta(He/N_2)$ after the analysis if O_2/N_2, Ar/N_2, and CO_2 concentrations of the sample are determined as well. An online getter preconcentrates He and other noble gases before entry into the MS by chemically removing >99.99 % of all N_2 and O_2 in a reaction with titanium sponge. Our method thereby avoids the need for peak jumping and avoids the need for a multi-collector mass spectrometer, while achieving a precision of ~10 per meg (1σ) on repeat analysis of $\delta(He/N_2)$ in high pressure tanks.

In future work, the gettering and flow-stabilizing inlet system could be used to investigate possible interannual to decadal changes in stratospheric $\delta(He/N_2)$ linked to variability in stratospheric circulation and stratosphere-troposphere exchange processes. Additional applications could include the search for a signal of anthropogenic helium release during fossil fuel extraction and burning (Boucher et al., 2018c; Lupton and Evans, 2013, 2004; Mabry et al., 2015; Oliver et al., 1984; Pierson-Wickmann et al., 2001; Sano et al., 1989), or measurements of spatial gradients resulting from localized human or natural sources of helium (Boucher et al., 2018a, 2018b; Sano et al., 2010). The setup is also suitable for the analysis of other noble gases and could therefore be used to study seasonal ocean warming associated with degassing or uptake of Kr and Xe from the ocean (Baggenstos et al., 2019; Bereiter et al., 2018).

6 Acknowledgements

We thank Ross Beaudette, Alan Seltzer, Sarah Shackleton, Jacob Morgen, Jessica Ng, and Eric Morgan for laboratory support and insightful discussions during the development of the He/N_2 analysis system. We are grateful to Shane Clark, Savannah Hatley, Adam Cox, and Timothy Lueker for providing high-pressure cylinders used during testing. We also thank them for maintaining and operating the Ar/N_2, O_2/N_2 and CO_2 analysis systems in the Keeling laboratory. This work was supported by the National Science Foundation grants MRI-1920369 and AGS-1940361.

7 Data availability

Data presented in this manuscript are available as an electronic supplement to this paper from the journal website.

8 Competing interests

The authors declare that they have no conflict of interest.

9 Author contribution

BB designed and build the inlet system with important design expertise from WP, JS and RK. BB performed all testing and prepared the manuscript with contributions from all co-authors.

10 References

Arblaster, J.M., Gillett, N.P., Calvo, N., Forster, P.M., Polvani, L.M., Son, S.-W., Waugh, D.W., Young, P.J., 2014. Stratospheric ozone changes and climate, Chapter 4, Scientific Assessment of Ozone Depletion: 2014, Global Ozone Research and Monitoring Project – Report No. 55. Geneva, Switzerland.

Baggenstos, D., Häberli, M., Schmitt, J., Shackleton, S.A., Birner, B., Severinghaus, J.P., Kellerhals, T., Fischer, H., 2019. Earth's radiative imbalance from the Last Glacial Maximum to the present. Proceedings of the National Academy of Sciences of the United States of America 116, 14881–14886. https://doi.org/10.1073/pnas.1905447116

Belikov, D., Sugawara, S., Ishidoya, S., Hasebe, F., Maksyutov, S., Aoki, S., Morimoto, S., Nakazawa, T., 2019. Three-dimensional simulation of stratospheric gravitational separation using the NIES global atmospheric tracer transport model. Atmospheric Chemistry and Physics 19, 5349–5361. https://doi.org/10.5194/acp-19-5349-2019

Bereiter, B., Shackleton, S., Baggenstos, D., Kawamura, K., Severinghaus, J., 2018. Mean global ocean temperatures during the last glacial transition. Nature 553, 39–44. https://doi.org/10.1038/nature25152

Birner, B., Chipperfield, M.P., Morgan, E.J., Stephens, B.B., Linz, M., Feng, W., Wilson, C., Bent, J.D., Wofsy, S.C., Severinghaus, J., Ralph, F., 2020. Gravitational separation of Ar/N2 and age of air in the lowermost stratosphere in airborne observations and a chemical transport model. Atmospheric Chemistry and Physics Discussions 1–34. https://doi.org/https://doi.org/10.5194/acp-2020-95

Bönisch, H., Engel, A., Curtius, J., Birner, T., Hoor, P., 2009. Quantifying transport into the lowermost stratosphere using simultaneous in-situ measurements of SF6 and CO2. Atmospheric Chemistry and Physics 9, 5905–5919. https://doi.org/10.5194/acp-9-5905-2009

Boucher, C., Lan, T., Mabry, J., Bekaert, D. V., Burnard, P.G., Marty, B., 2018a. Spatial analysis of the atmospheric helium isotopic composition: Geochemical and environmental implications. Geochimica et Cosmochimica Acta 237, 120–130.

https://doi.org/10.1016/j.gca.2018.06.010

Boucher, C., Lan, T., Marty, B., Burnard, P.G., Fischer, T.P., Ayalew, D., Mabry, J., Maarten de Moor, J., Zelenski, M.E., Zimmermann, L., 2018b. Atmospheric helium isotope composition as a tracer of volcanic emissions: A case study of Erta Ale volcano, Ethiopia. Chemical Geology 480, 3–11. https://doi.org/10.1016/j.chemgeo.2017.05.011

Boucher, C., Marty, B., Zimmermann, L., Langenfelds, R., 2018c. Atmospheric helium isotopic ratio from 1910 to 2016 recorded in stainless steel containers. Geochemical Perspectives Letters 6, 23–27. https://doi.org/10.7185/geochemlet.1804

Brewer, A.W., 1949. Evidence for a world circulation provided by the measurements of helium and water vapour distribution in the stratosphere. Quarterly Journal of the Royal Meteorological Society 75, 351–363. https://doi.org/10.1002/qj.49707532603

Butchart, N., 2014. The Brewer-Dobson circulation. Reviews of Geophysics 52, 157–184. https://doi.org/10.1002/2013RG000448

Dobson, G.M.B., 1956. Origin and distribution of the polyatomic molecules in the atmosphere. Proceedings of the Royal Society of London. Series A. Mathematical and Physical Sciences 236, 187–193. https://doi.org/10.1098/rspa.1956.0127

Engel, A., Bönisch, H., Ullrich, M., Sitals, R., Membrive, O., Danis, F., Crevoisier, C., 2017. Mean age of stratospheric air derived from AirCore observations. Atmospheric Chemistry and Physics 17, 6825–6838. https://doi.org/10.5194/acp-17-6825-2017

Engel, A., Möbius, T., Bönisch, H., Schmidt, U., Heinz, R., Levin, I., Atlas, E., Aoki, S., Nakazawa, T., Sugawara, S., Moore, F., Hurst, D., Elkins, J., Schauffler, S., Andrews, A., Boering, K., 2009. Age of stratospheric air unchanged within uncertainties over the past 30 years. Nature Geoscience 2, 28–31. https://doi.org/10.1038/ngeo388

Flury, T., Wu, D.L., Read, W.G., 2013. Variability in the speed of the Brewer-Dobson circulation as observed by Aura/MLS. Atmospheric Chemistry and Physics 13, 4563–4575. https://doi.org/10.5194/acp-13-4563-2013

Fowler, D., Coyle, M., Skiba, U., Sutton, M.A., Cape, J.N., Reis, S., Sheppard, L.J., Jenkins, A., Grizzetti, B., Galloway, J.N., Vitousek, P., Leach, A., Bouwman, A.F., Butterbach-Bahl, K., Dentener, F., Stevenson, D., Amann, M., Voss, M., 2013. The global nitrogen cycle in the Twentyfirst century. Philosophical Transactions of the Royal Society B: Biological Sciences 368. https://doi.org/10.1098/rstb.2013.0164

Glückauf, E., 1944. A simple analysis of the helium content of air. Transactions of the Faraday Society 44, 436–439.

Graven, H.D., Guilderson, T.P., Keeling, R.F., 2012. Observations of radiocarbon in CO2 at La Jolla, California, USA 1992-2007: Analysis of the long-term trend. Journal of Geophysical Research Atmospheres 117, 1–14. https://doi.org/10.1029/2011JD016533

Haenel, F.J., Stiller, G.P., Von Clarmann, T., Funke, B., Eckert, E., Glatthor, N., Grabowski, U., Kellmann, S., Kiefer, M., Linden, A., Reddmann, T., 2015. Reassessment of MIPAS age of air trends and variability. Atmospheric Chemistry and Physics 15, 13161–13176. https://doi.org/10.5194/acp-15-13161-2015

Hamilton, K., Fan, S.-M., 2000. Effects of the stratospheric quasi-biennial oscillation on long-lived greenhouse gases in the troposphere. Journal of Geophysical Research 105, 20581. https://doi.org/10.1029/2000JD900331

Hamme, R.C., Emerson, S.R., 2004. The solubility of neon, nirogen and argon in distilled water and seawater. Deep-Sea Research I 51, 1517–1528.

Hegglin, M.I., Shepherd, T.G., 2009. Large climate-induced changes in ultraviolet index and stratosphere-to- troposphere ozone flux. Nature Geoscience 2, 687–691. https://doi.org/10.1038/ngeo604

Henneberg, D., Heinrichs, U., Schomburg, G., 1975. Open Split Connection of Glass Capillary Columns to Mass Spectrometers. Chromatographia 8, 449–451.

Holton, J.R., Haynes, P.H., Mcintyre, M.E., Douglass, A.R., Rood, B., 1995. Stratosphere-Troposphere. Review of Geophysics 403–439.

Ishidoya, S., Sugawara, S., Inai, Y., Morimoto, S., Honda, H., Ikeda, C., Hashida, G., Machida, T., Tomikawa, Y., Toyoda, S., Goto, D., Aoki, S., Nakazawa, T., 2018. Gravitational separation of the stratospheric air over Syowa, Antarctica and its connection with meteorological fields. Atmospheric Science Letters 19, 1–7. https://doi.org/10.1002/asl.857

Ishidoya, S., Sugawara, S., Morimoto, S., Aoki, S., Nakazawa, T., 2008. Gravitational separation of major atmospheric components of nitrogen and oxygen in the stratosphere. Geophysical Research Letters 35. https://doi.org/10.1029/2007GL030456

Ishidoya, S., Sugawara, S., Morimoto, S., Aoki, S., Nakazawa, T., Honda, H., Murayama, S., 2013. Gravitational separation in the stratosphere - A new indicator of atmospheric circulation. Atmospheric Chemistry and Physics 13, 8787–8796. https://doi.org/10.5194/acp-13-8787-2013

Ishidoya, S., Sugawara, S., Tohjima, Y., Goto, D., Ishijima, K., Niwa, Y., Aoki, N., Murayama, S., 2020. Secular change of the atmospheric Ar/N2 and its implications for ocean heat uptake and Brewer-Dobson circulation. Atmospheric Chemistry and Physics Discussions. https://doi.org/doi.org/10.5194/acp-2020-301

Jenkins, W.J., Lott, D.E., Cahill, K.L., 2019. A determination of atmospheric helium, neon, argon, krypton, and xenon solubility concentrations in water and seawater. Marine Chemistry 211, 94–107. https://doi.org/10.1016/j.marchem.2019.03.007

Keeling, R.F., 1988. Development of an interferometric oxygen analyzer for precise measurement of the atmospheric O2 mole fraction. Harvard University.

Keeling, R.F., Blaine, T., Paplawsky, B., Katz, L., Atwood, C., Brockwell, T., 2004. Measurement of changes in atmospheric Ar/N_2 ratio using a rapid-switching, single-capillary mass spectrometer system. Tellus 56B, 322–338. https://doi.org/10.1111/j.1600-0889.2004.00117.x

Keeling, R.F., Manning, A.C., McEvoy, E.M., Shertz, S.R., 1998. Methods for measuring changes in atmospheric O2 concentration and their application in southern hemisphere air. Journal of Geophysical Research 103, 3381–3397. https://doi.org/10.1029/97JD02537

Keeling, R.F., Manning, A.C., Paplawsky, W.J., Cox, A.C., 2007. On the long-term stability of reference gases for atmospheric O2/N2 and CO2 measurements. Tellus B: Chemical and Physical Meteorology 59B, 3–14.

https://doi.org/10.5194/amt-2020-313
Preprint. Discussion started: 15 September 2020

https://doi.org/10.1111/j.1600-0889.2006.00196.x

Kockarts, G., 1973. Helium in the terrestrial atmosphere. Space Science Reviews 14, 723–757. https://doi.org/10.1007/BF00224775

Li, F., Waugh, D.W., Douglass, A.R., Newman, P.A., Pawson, S., Stolarski, R.S., Strahan, S.E., Nielsen, J.E., 2012. Seasonal variations of stratospheric age spectra in the Goddard Earth Observing System Chemistry Climate Model (GEOSCCM). Journal of Geophysical Research Atmospheres 117, 1–14. https://doi.org/10.1029/2011JD016877

Lupton, J., Evans, L., 2013. Changes in the atmospheric helium isotope ratio over the past 40 years. Geophysical Research Letters 40, 6271–6275. https://doi.org/10.1002/2013GL057681

Lupton, J., Evans, L., 2004. The atmospheric helium isotope ratio: Is it changing? Geophysical Research Letters 31, 1–4. https://doi.org/10.1029/2004GL020041

Mabry, J.C., Lan, T., Boucher, C., Burnard, P.G., Brennwald, M.S., Langenfelds, R., Marty, B., 2015. No evidence for change of the atmospheric helium isotope composition since 1978 from re-analysis of the Cape Grim Air Archive. Earth and Planetary Science Letters 428, 134–138. https://doi.org/10.1016/j.epsl.2015.07.035

Montzka, S.A., Dutton, G.S., Yu, P., Ray, E., Portmann, R.W., Daniel, J.S., Kuijpers, L., Hall, B.D., Mondeel, D., Siso, C., Nance, J.D., Rigby, M., Manning, A.J., Hu, L., Moore, F., Miller, B.R., Elkins, J.W., 2018. An unexpected and persistent increase in global emissions of ozone-depleting CFC-11. Nature 557, 413–417. https://doi.org/10.1038/s41586-018-0106-2

Nevison, C.D., Dlugokencky, E., Dutton, G., Elkins, J.W., Fraser, P., Hall, B., Krummel, P.B., Langenfelds, R.L., O’Doherty, S., Prinn, R.G., Steele, L.P., Weiss, R.F., 2011. Exploring causes of interannual variability in the seasonal cycles of tropospheric nitrous oxide. Atmospheric Chemistry and Physics 11, 3713–3730. https://doi.org/10.5194/acp-11-3713-2011

Oliver, B.M., Bradley, J.G., Farrar IV, H., 1984. Helium concentration in the Earth’s lower atmosphere. Geochimica et Cosmochimica Acta 48, 1759–1767. https://doi.org/10.1016/0016-7037(84)90030-9

Pierson-Wickmann, A.C., Marty, B., Ploquin, A., 2001. Helium trapped in historical slags: A search for temporal variation of the He isotopic composition of air. Earth and Planetary Science Letters 194, 165–175. https://doi.org/10.1016/S0012-821X(01)00554-4

Ray, E.A., Moore, F.L., Rosenlof, K.H., Davis, S.M., Boenisch, H., Morgenstern, O., Smale, D., Rozanov, E., Hegglin, M., Pitari, G., Mancini, E., Braesicke, P., Butchart, N., Hardiman, S., Li, F., Shibata, K., Plummer, D.A., 2010. Evidence for changes in stratospheric transport and mixing over the past three decades based on multiple data sets and tropical leaky pipe analysis. Journal of Geophysical Research Atmospheres 115, 1–16. https://doi.org/10.1029/2010JD014206

Ray, E.A., Moore, F.L., Rosenlof, K.H., Davis, S.M., Sweeney, C., Tans, P., Wang, T., Elkins, J.W., Bönisch, H., Engel, A., Sugawara, S., Nakazawa, T., Aoki, S., 2014. Improving stratospheric transport trend analysis based on SF6 and CO2 measurements. Journal of Geophysical Research: Atmospheres 119, 14110–14128. https://doi.org/10.1002/2014JD021802

Reid, R.C., Prausnitz, J.M., Poling, B.E., 1987. The properties of gases and liquids, 4th ed. McGraw-Hill, New York.

Salby, M.L., Callaghan, P.F., 2006. Influence of the Brewer-Dobson circulation on stratosphere-troposphere exchange. Journal of Geophysical Research Atmospheres 111, 1–9. https://doi.org/10.1029/2006JD007051

Sano, Y., Furukawa, Y., Takahata, N., 2010. Atmospheric helium isotope ratio: Possible temporal and spatial variations. Geochimica et Cosmochimica Acta 74, 4893–4901. https://doi.org/10.1016/j.gca.2010.06.003

Sano, Y., Marty, B., Burnard, P., 2013. Noble Gases in the Atmosphere, in: Burnard, P. (Ed.), The Noble Gases as Geochemical Tracers. Springer Berlin Heidelberg, pp. 17–31. https://doi.org/10.1007/978-3-642-28836-4_2

Sano, Y., Wakita, H., Makide, Y., Tominaga, T., 1989. A ten-year decrease in the atmospheric helium isotope ratio possibly caused by human activity. Geophysical Research Letters 16, 1371–1374. https://doi.org/10.1029/GL016i012p01371

Simmonds, P.G., Manning, A.J., Athanassiadou, M., Scaife, A.A., Derwent, R.G., O'Doherty, S., Harth, C.M., Weiss, R.F., Dutton, G.S., Hall, B.D., Sweeney, C., Elkins, J.W., 2013. Interannual fluctuations in the seasonal cycle of nitrous oxide and chlorofluorocarbons due to the Brewer-Dobson circulation. Journal of Geophysical Research Atmospheres 118, 10694–10706. https://doi.org/10.1002/jgrd.50832

Sugawara, S., Ishidoya, S., Aoki, S., Morimoto, S., Nakazawa, T., Toyoda, S., Inai, Y., Hasebe, F., Ikeda, C., Honda, H., Goto, D., Putri, F.A., 2018. Age and gravitational separation of the stratospheric air over Indonesia. Atmospheric Chemistry and Physics 18, 1819–1833. https://doi.org/10.5194/acp-18-1819-2018

Torgersen, T., 1989. Terrestrial helium degassing fluxes and the atmospheric helium budget: Implications with respect to the degassing processes of continental crust. Chemical Geology: Isotope Geoscience Section 79, 1–14. https://doi.org/10.1016/0168-9622(89)90002-X

Weiss, R.F., 1971. Solubility of helium and neon in water and seawater. Journal of Chemical & Engineering Data 16, 235–241. https://doi.org/10.1021/je60049a019

Zartman, R.E., Wasserburg, G.J., Reynolds, J.H., 1961. Helium, Argon, and Carbon in Some Natural Gases. Journal of Geophysical Research 66, 277–306. https://doi.org/10.1029/jz066i001p00277

https://doi.org/10.5194/amt-2020-313
Preprint. Discussion started: 15 September 2020

Atmospheric Measurement Techniques
Discussions

11 Figures and Figure Captions

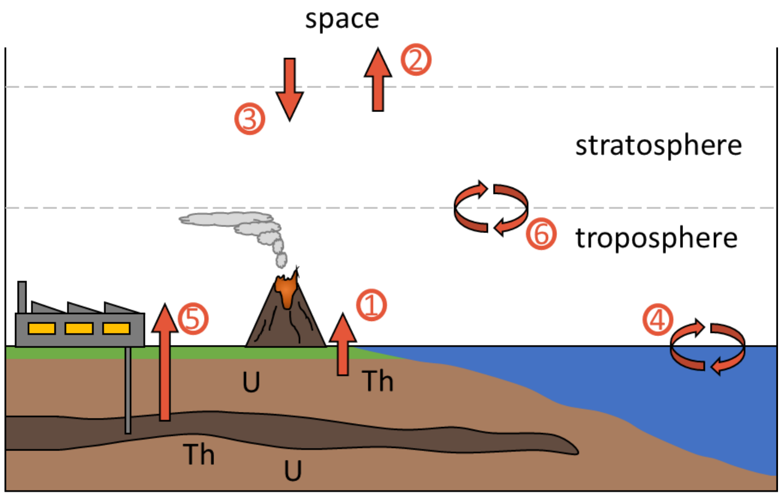

Figure 1. Schematic depiction of ^{4}He fluxes to and from the troposphere. Different processes are numbered and listed in Table 1.

https://doi.org/10.5194/amt-2020-313
Preprint. Discussion started: 15 September 2020

Atmospheric Measurement Techniques
Discussions

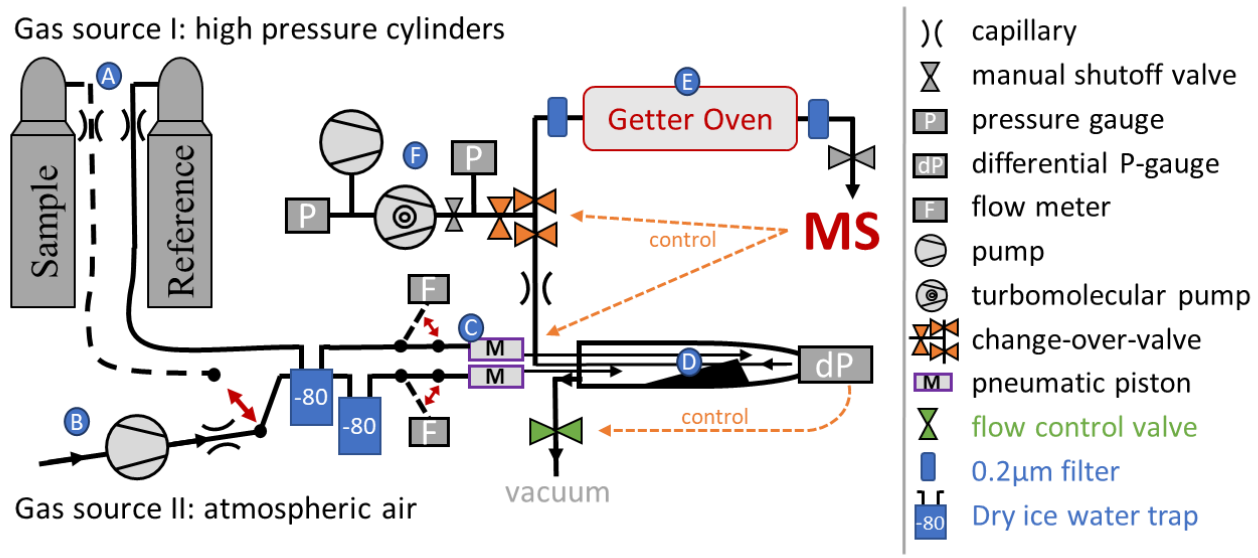

Figure 2. Schematic depiction of the flow-stabilizing MS inlet system. Dashed orange arrows highlighted important control pathways and letters A-F in blue circles label the main sections of the inlet system. Red double arrows indicate manual switching option in the inlet system. Gas can either be delivered from samples in high-pressure cylinders (A) or locally pumped ambient air (B). The flow can be measured by two Omron flow meters before entry into the pressure stabilization chamber (C). Pistons (D) alternatingly move fine metal tubing in the pressure stabilization chamber pushing either the sample or standard gas stream deeper into the stabilization chamber where the gas will be picked up by a single capillary leading to the MS. The chamber is exhausted to a vacuum system and the pressure is monitored and controlled by a differential pressure gauge combined with an automatic MKS flow control valve. The stainless-steel getter oven (E) has an inner diameter of 1/2" and is filled with 10–12 g of titanium sponge. 2µm-filters prevent particles from contaminating the MS and gas delivery system. In case of an anomalous pressure change in the MS or when venting the getter oven, the getter oven can be isolated from the pressure-stabilization chamber with a change-over-valve controlled directly by the MS software. The entire inlet vacuum system is backed by a diaphragm vacuum pump and a turbomolecular pump (F). A manual shutoff-valve can isolate the getter oven from the MS.

https://doi.org/10.5194/amt-2020-313
Preprint. Discussion started: 15 September 2020

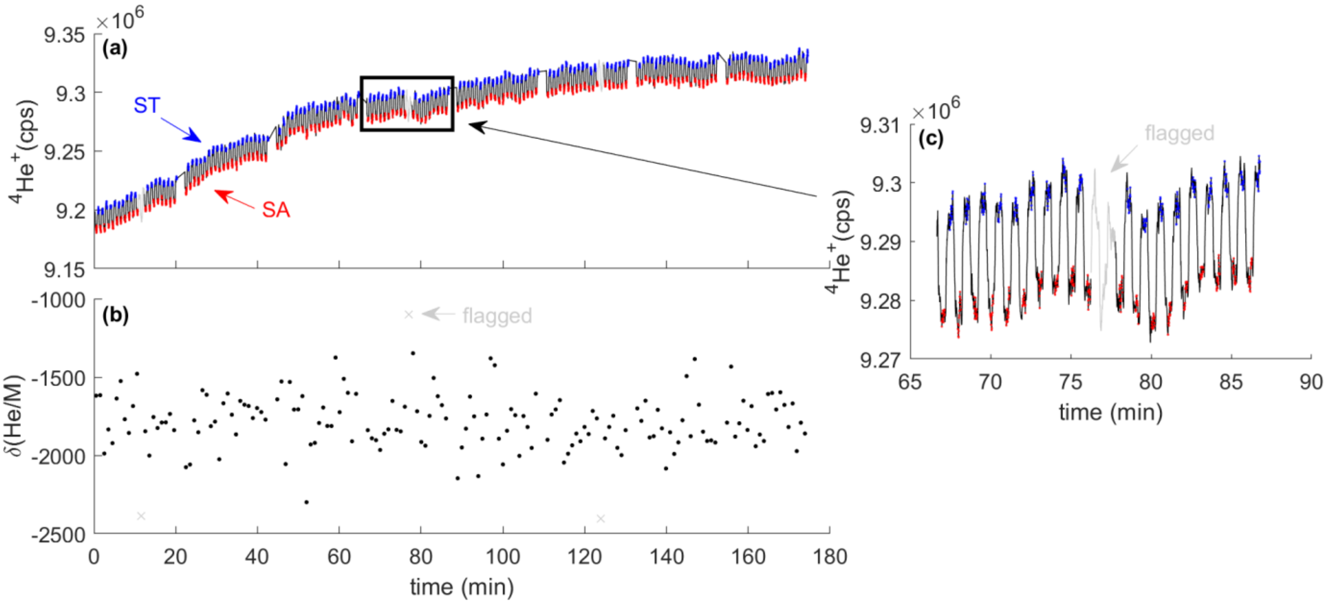

Figure 3. Typical analysis results from the measurement of two high pressure cylinders. The MS monitors the $^4He^+$-ion beam during switching between sample (SA) and standard (ST) gas (a). Red and blue shaded data points highlight the periods used for integration and calculation of the delta value (b). They are separated by idle times (black lines) to allow complete flushout after switching. Data are quality controlled and flagged periods are shown in grey. Inset (c) shows one block of 20 sample-standard comparisons including one cycled that was flagged as an outlier.

https://doi.org/10.5194/amt-2020-313
Preprint. Discussion started: 15 September 2020

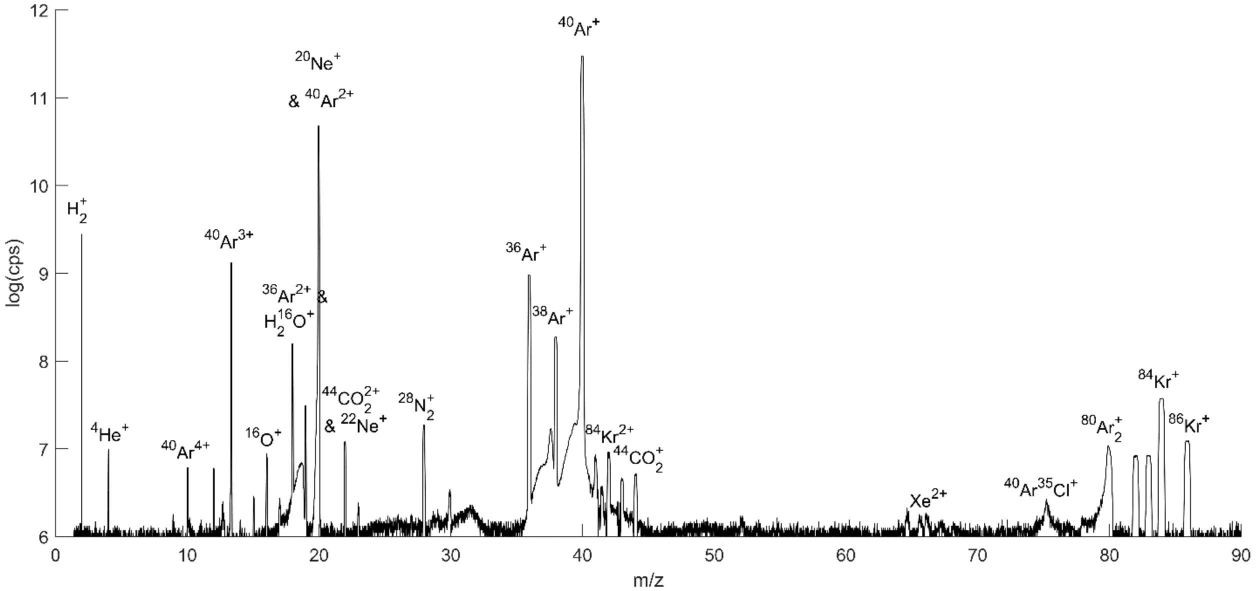

Figure 4. Mass scan of ambient air. Ion beam intensity is shown as the logarithm of the ions counted per second, and select ion species are labeled.

https://doi.org/10.5194/amt-2020-313
Preprint. Discussion started: 15 September 2020

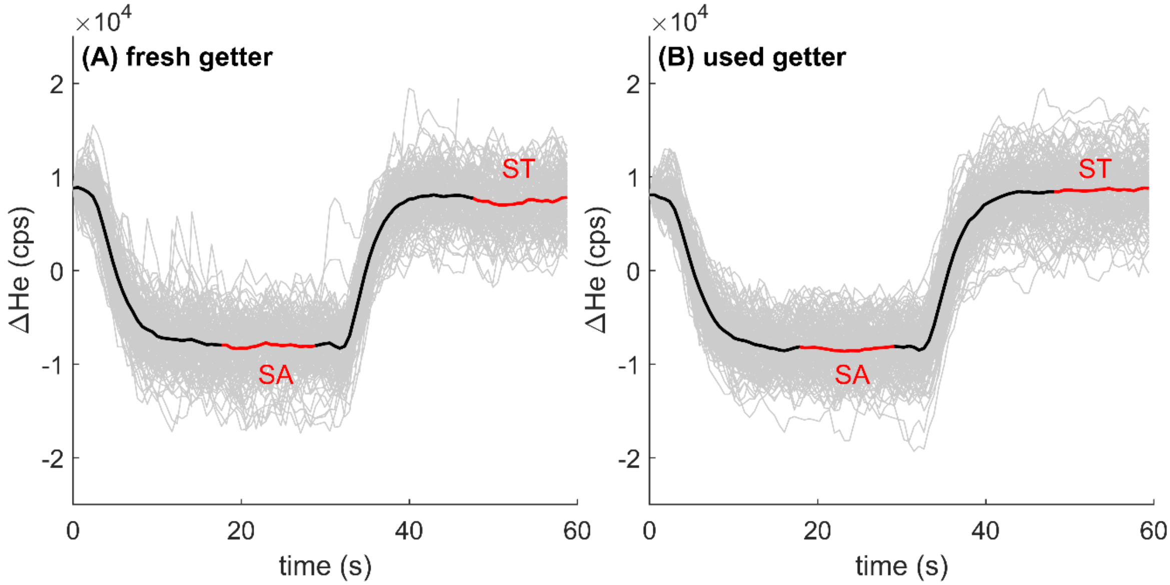

470 **Figure 5.** Stack of ^{4}He ion count difference (10^4 counts per second, cps) when switching between the same standard (ST) and sample (SA) gas stream using fresh titanium sponge (A) and nearly depleted getter material (B). Grey lines show individual records forced to align at time equals zero and the thick black line shows the average of all stacked switching events. The analysis cycle consists of (i) switching to SA with an idle time of ~18 seconds, (ii) a ~12 second integration of ions from SA, (iii) switching back to ST, again with a ~18 second idle time, and finally (iiii) a ~12 second integration of ST.

https://doi.org/10.5194/amt-2020-313
Preprint. Discussion started: 15 September 2020

Atmospheric Measurement Techniques Discussions

475

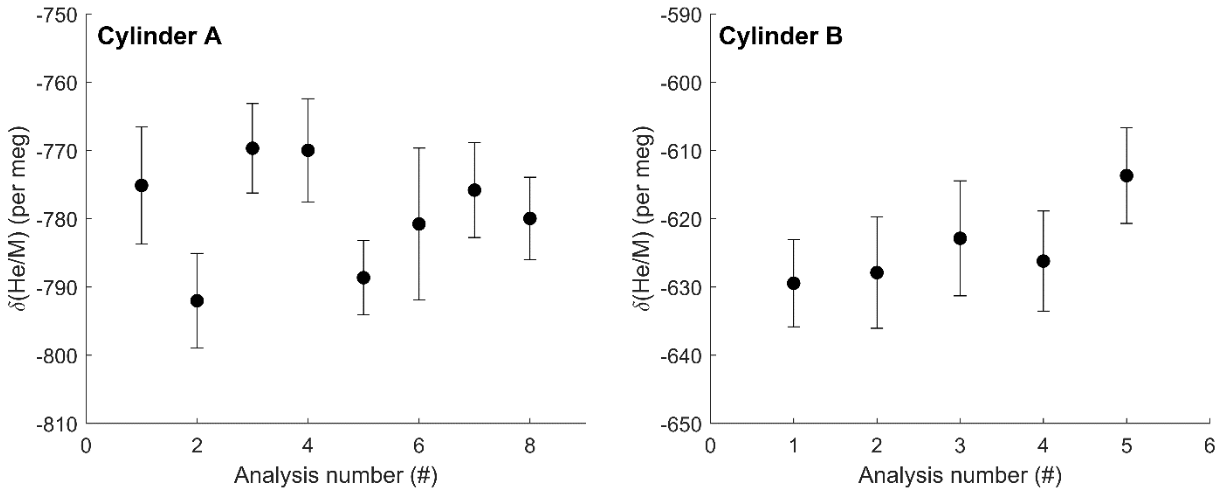

Figure 6. Repeat δ(He/M) measurement of two high-pressure cylinders against ambient La Jolla air collected in 2019. Repeat analysis show a standard deviation of 8.1 and 6.3 per meg for cylinder A and cylinder B respectively. Analysis 6 for cylinder A was shorter resulting in a larger uncertainty for that measurement. Data are not corrected for zero enrichment effects discussed in the text.

https://doi.org/10.5194/amt-2020-313
Preprint. Discussion started: 15 September 2020

Atmospheric Measurement Techniques Discussions

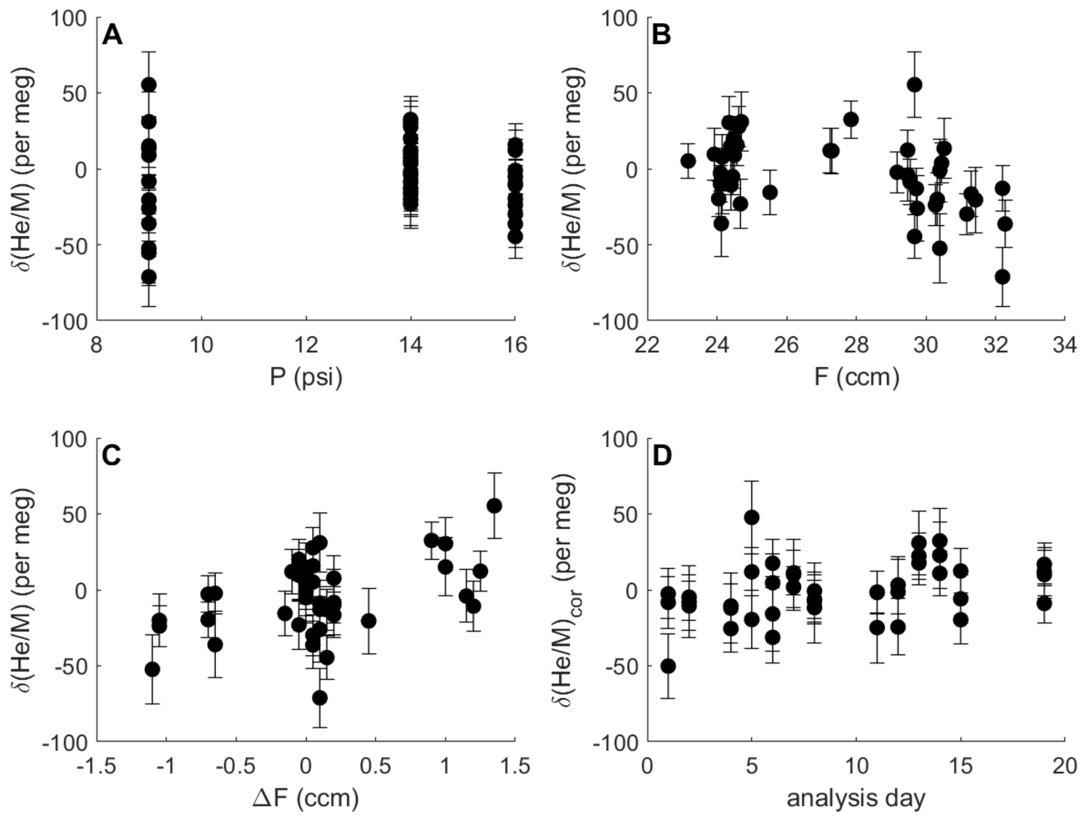

Figure 7. Difference in δ(He/M) between two identical gas streams (i.e., the zero enrichment) measured repeatedly under different conditions over 1.5–3h. Error bars show 1σ uncertainty. Measurements were made at different pressure levels (a), with slightly varying gas flows to the stabilization chamber (b), and imbalances in flow between SA and ST side (c). The same shared capillary was used for all analysis. Therefore, the pressure in the stabilization chamber controls the intensity of the ion beam and the internal precision of the analysis, illustrated by the greater scatter of observations at 9 psi (62.1 kPa). Delta values shown in (d) were corrected for the influence of pressure, mean flow, and flow imbalance according to coefficients found by multiple linear regression (see text). For a pressure of 14 psi (96.5 kPa), corrected delta values generally show scatter as expected from shot-noise behavior and corrected delta values are stable over time.

https://doi.org/10.5194/amt-2020-313
Preprint. Discussion started: 15 September 2020

12 Tables and Table Captions

490 **Table 1.** Processes contributing to variations in the tropospheric and stratospheric $^4He/N_2$ ratio.

Process	**^4He flux (10^7 mol y^{-1})**	**Tropospheric $\delta(^4He/N_2)$ trend[1] (per meg y^{-1})**	**Stratospheric $\delta(^4He/N_2)$ trend[1] (per meg y^{-1})**	**Tropospheric $\delta(^4He/N_2)$ anomaly (per meg)**	**Reference[2]**
Long-term trend					
(1) Crustal degassing and volcanism	24.0–50.7	0.26–0.55			(a)
(2) Loss to space	53.3–106.8	-0.58–-1.15			(a,b)
(3) Non-terrestrial sources	insignificant	-			(a)
(4) Global Ocean warming[3]	1.3	-0.16			
(5) Fossil fuel extraction[4]	3189–12755 13000±7000 34000	34–138 140±76 367			(c) (d) (e)
(6) BDC acceleration[5]		0.5	-15		
Observational limits on decadal trends[6]		-1.4±44.5 9.5±32.7 -2±23.8			(f) (g) (h)
Seasonal and interannual variability					
Seasonal cycle of global ocean heat[7]				3–9	
Strat. circ. & STE variability[8]		±6	±375		
Interhemispheric difference[9]				<30	

[1] $\delta(^4He/N_2)$ trends are calculated using first column and assuming total atmospheric ^4He = 9.268 e+14 mol. N_2 changes are generally neglected except for ocean degassing. Tropospheric trends are globally uniform because the troposphere is well mixed. Stratospheric trend estimates are given for 35km in the mid latitude Northern Hemisphere.

[2] (a) Torgersen (1989)
(b) Kockarts (1973)
(c) Oliver et al. (1984)
(d) Pierson-Wickmann et al. (2001)
(e) Sano et al. (2013)
(f) Lupton and Evans (2013)
(g) Mabry et al. (2015)
(h) Boucher et al. (2018c)

[3] calculated from ^4He and N_2 solubility changes (Weiss, 1971; Hamme and Emerson, 2004) for an ocean heat content trend of 10ZJ y^{-1} at a mean water temperature of 10°C.

[4] (c) includes natural gas, coal and uranium, (d) and (e) include natural gas, petroleum and coal.

[5] $\delta(^4He/N_2)$ rescaled from $\delta(Ar/N_2)$ assuming 7.5x greater gravitational separation. The secular $\delta(Ar/N_2)$ trend was simulated in the SOCRATES model for an accelerating BDC scenario (+4 % dec^{-1}) by Ishidoya et al. (2020). $\delta(^4He/N_2)$ trend is adjusted to reflect a more plausible BDC acceleration of +2 % dec^{-1}.

[6] observed $^3He/^4He$ trends are translated to ^4He trends assuming $^3He/^4He$ = 3e-8 in fossil fuel associated helium.

[7] scaled from seasonal $\delta(Ar/N_2)$ changes of 5-15 per meg (Keeling et al., 2004) using solubility-temperature dependency of He, N_2 and Ar in a 10°C warm surface ocean (Weiss, 1971; Hamme and Emerson, 2004).

[8] Tropospheric and stratospheric $\delta(^4He/N_2)$ rescaled from $\delta(Ar/N_2)$. Ishidoya et al. (2020) report a ±0.4 and ±25 per meg $\delta(Ar/N_2)$ change in troposphere and stratosphere in the SOCRATES model for a sinusoidal ±5% change in BDC strength over 3 years.

https://doi.org/10.5194/amt-2020-313
Preprint. Discussion started: 15 September 2020

Atmospheric Measurement Techniques Discussions

[9] Assuming that industrial He release is confined to the Northern Hemisphere and assuming an annual $\delta(^{4}He/N_2)$ increase of ~30 per meg (consistent with the current observational error) yields an interhemispheric $\delta(^{4}He/N_2)$ difference < 30 per meg. Differences in STE of He between the hemispheres are neglected here but could be important.

https://doi.org/10.5194/amt-2020-313
Preprint. Discussion started: 15 September 2020

Atmospheric Measurement Techniques Discussions

Table 2. Summary of observed ion beams in Figure 4. Relative ion beam intensities on MAT253 are calculated from the scan with identical source tuning. Xe isotope beams were not observed but scaled from previous observations in the lab.

m/z	Dominant ions	Ion beam intensity (cps)*	ion beam intensity relative to He^+
4	$^{4}He^{+}$	9.70E+06	1
20	$^{20}Ne^{+}$,$^{40}Ar^{2+}$	4.78E+10	4916.1
22	$^{22}Ne^{+}$,$^{44}CO_2^{2+}$	1.22E+07	1.25
36	$^{36}Ar^{+}$	9.55E+08	98.26
38	$^{38}Ar^{+}$	1.89E+08	19.44
40	$^{40}Ar^{+}$	2.98E+11	30660
82	$^{82}Kr^{+}$	8.50E+06	0.87
83	$^{83}Kr^{+}$	8.40E+06	0.86
84	$^{84}Kr^{+}$	3.76E+07	3.87
86	$^{86}Kr^{+}$	1.22E+07	1.25
129*	$^{129}Xe^{+}$	2.60E+06	0.27
131*	$^{131}Xe^{+}$	2.10E+06	0.22
132*	$^{132}Xe^{+}$	2.70E+06	0.28
136*	$^{136}Xe^{+}$	9.00E+05	0.09

*Xe isotopes were not measured directly here because of the limited dynamic range of the MAT 253 when set to measure He. Instead we report expected Xe ion beam intensities scaled from previously analysis of Kr and Xe in the lab assuming natural isotopic abundances.